www.nature.com/aps

Acta Pharmacologica Sinica

ARTICLE

Pyrazolone derivative C29 protects against HFD-induced obesity in mice via activation of AMPK in adipose tissue

Bo-han Li[1,2], Mei Zhang[1], Ya-nan Duan[1], Lin Shuai[1], Hao-wen Jiang[1], Jia Li[1,2], Fa-jun Nan[1] and Jing-ya Li[1]

Beige adipocytes have been considered as a potential strategy in anti-obesity therapy because of its thermogenic capacity. AMP-activated protein kinase (AMPK) plays important roles in regulating adipose tissue function. C29 is a novel pyrazolone derivative with AMPK activity. In the current study, we investigated the role of C29 in the regulation of thermogenesis using differentiated adipocytes and diet-induced obese mice, and explored the mechanisms that might be involved in energy expenditure via adipocyte AMPK activation. We showed that treatment with C29 (2.5–10 μM) concentration-dependently increased thermogenesis in differentiated preadipocytes separated from inguinal white adipose tissue (iWAT), evidenced by increased expression levels of thermogenesis markers such as *Ucp1*, *Pgc-1α*, *Dio2*, *Prdm16*, *Cox7a1*, *Cox8b*, *Elovl3,* and *Cidea*, fatty acid oxidation (FAO) genes including *Cpt1a*, *Lcad* and *Ppara*, as well as beige-selective genes such as *Cd137*, *Tmem26*, *Slc27a1,* and *Tbx1*. In high-fat diet (HFD)-fed mice, oral administration of C29 (30 $mg{\cdot}kg^{-1}{\cdot}day^{-1}$) for 9 weeks alleviated HFD-induced obesity, promoted energy expenditure and modulated iWAT browning. However, these effects were not observed in adipose-specific AMPKα1/α2 knockout (AKO) mice following C29 administration. Together, this study demonstrates that C29 regulates energy balance via adipocyte AMPK. Our findings show that the discovery of AMPK activators that specifically target adipose tissue may have therapeutic potential for treating obesity-related metabolic diseases.

Keywords: AMP-activated protein kinase; pyrazolone derivative C29; obesity; energy expenditure; thermogenesis; inguinal white adipose tissue; white adipose browning

Acta Pharmacologica Sinica (2021) 42:964–974; https://doi.org/10.1038/s41401-020-00524-0

INTRODUCTION

Obesity has become one of the most serious global health problems and has been found to lead to an increased risk of type 2 diabetes, cardiovascular diseases, nonalcoholic fatty liver disease, and several forms of cancer [1]. Therefore, weight-loss treatments have become an urgent need. The main cause of the development of obesity is the imbalance between energy intake and energy consumption. Adipose tissues, which consist mainly of adipocytes, are important in controlling whole-body energy homeostasis [2, 3]. Traditionally, adipocytes can be broadly divided into white and brown fat cells. While white fat cells are highly adapted to storing excess energy in the form of triglycerides, brown adipocytes oxidize chemical energy to produce heat, a process called nonshivering thermogenesis that counteracts hypothermia, obesity, and diabetes. Brown adipocytes, which have multilocular morphology, have a relatively high mitochondrial content and high mitochondrial uncoupling protein 1 (UCP1) expression [4–6]. Recently, it was discovered that a new type of adipocyte, known as beige adipocytes, arises in white adipose tissue under stimulus conditions. Beige adipocytes have a low basal level of uncoupling protein 1 (UCP1), but it can be induced to levels similar to classical brown adipocytes when responding to cold or hormonal stimuli and soon afterwards activates a thermogenic program [7–9]. Burning off excess heat through classical brown and beige fat cells can increase whole-body energy expenditure [10, 11].

In recent years, effective ways to promote thermogenic activity through brown adipose tissue (BAT) or the browning of inguinal white adipose tissue (iWAT) have been of great interest as potential therapeutics for anti-obesity treatments. Studies have revealed that brown/beige adipocytes respond to thermogenic stimuli, such as irisin [12], fibroblast growth factor 21 (FGF21) [13], natriuretic peptides [14], bone morphogenic proteins (BMPs) 4 and 7 [15, 16] and the peroxisome proliferator-activated receptor gamma (PPARγ) agonist rosiglitazone [17]. Therefore, new therapeutic strategies to counteract obesity and other metabolic diseases have enhanced the focus on these aspects.

AMP-activated protein kinase (AMPK), a ubiquitously distributed serine/threonine protein kinase, exists as multiple heterotrimeric complexes composed of a catalytic (α) subunit and two regulatory (β, γ) subunits [18, 19]. Essentially, conditions that lead to a rise in the AMP/ADP:ATP ratio cause an activation of AMPK through the increased phosphorylation of the α-subunit on Thr172 (T172) [20, 21]. Over the past years, it has been revealed that AMPK acts as a crucial cellular energy sensor and regulates whole-body nutrient metabolism. The activation of AMPK in the hypothalamus maintains energy balance by promoting food intake [22]. In addition to its crucial role in the central nervous system, AMPK

[1]State Key Laboratory of Drug Research, the National Drug Screening Center, Shanghai Institute of Materia Medica, Chinese Academy of Sciences, Shanghai 201203, China and [2]University of Chinese Academy of Sciences, Beijing 100049, China
Correspondence: Fa-jun Nan (fjnan@simm.ac.cn) or Jing-ya Li (jyli@simm.ac.cn)

Received: 17 April 2020 Accepted: 27 August 2020
Published online: 15 September 2020

also plays a key role in peripheral tissues. In the liver, AMPK suppresses hepatic gluconeogenesis and lipogenesis, while in skeletal muscle, AMPK stimulates glucose uptake and fatty acid oxidation [23]. Moreover, AMPK is required for fatty acid oxidation and nonshivering thermogenesis in adipose tissues [24]. Due to its vital role in regulating multiple tissue and metabolic pathways, AMPK has been considered a potential therapeutic target to alter metabolic syndrome.

In our previous study, we found a novel series of pyrazolone derivatives as direct nonselective AMPK activators in which C29 was selected as a typical compound because of its best AMPK activity ($EC_{50} = 2.1$ μmol/L, AMPK activity fold = 3.3). We highlighted that C29 directly activates the kinase domain of the AMPKα subunit, enabling the activation of different AMPK heterotrimers without subunit selectivity, and that it could be considered a novel allosteric AMPK activator. C29 increased the phosphorylation of AMPK without affecting the AMP/ATP and ADP/ATP ratios. Moreover, we identified that C29 administration significantly inhibited triglyceride accumulation in hepatocytes and improved lipid metabolism in the liver of *ob*/*ob* mice [25]. It is becoming increasingly evident that the increase in AMPK activity could result in the browning of WAT, and it may even enhance whole-body energy expenditure and have anti-obesity effects [26–30]. However, whether C29 influences energy balance or protects against high-fat diet (HFD)-induced obesity remains unclear. Therefore, the present study aimed to investigate the role of C29 in the regulation of energy expenditure using differentiated adipocytes and diet-induced obese mice, as well as to explore the mechanisms that might be involved in energy expenditure via adipocyte AMPK activation.

MATERIALS AND METHODS

Chemicals

C29 was synthesized as previously described [25]. Starting from ethyl 4-oxopiperidine-3-carboxylate hydrochloride and methyl 4-(bromomethyl) benzoate, five reaction steps were used to obtain C29. C29 was obtained as a yellow solid, purity 99.23%. For the in vitro study, C29 was dissolved in dimethyl sulfoxide (DMSO) at the indicated concentration. For the in vivo study, C29 was dissolved in 2% DMSO and 2% castor oil, which was then dissolved in 0.5% methylcellulose at the indicated concentration for oral animal administration.

Animals

All animal experiments were performed according to procedures approved by the Animal Care and Use Committee of the Shanghai Institute of Materia Medica. All animals were housed in a temperature-controlled room (22 ± 2 °C) with a 12-h light/dark cycle and ad libitum access to food and water. Six-week-old male C57BL/6 mice (Shanghai SLAC Laboratory Animal Co., Shanghai, China) were fed a high-fat diet (60% kCal from fat, D12492, Research Diets, New Brunswick, NJ, USA) for 8 weeks and then randomly assigned to treatment groups. Afterwards, mice were administered the vehicle (2% DMSO and 2% castor oil in 0.5% methylcellulose, p.o.) or C29 (30 $mg{\cdot}kg^{-1}{\cdot}day^{-1}$, p.o.) for 9 weeks. Body weight and food intake were measured every week. Adipose tissue-specific AMPKα1/α2 double-KO mice (referred to as AKO mice) were generated as previously described [31]. Beginning at 6 weeks of age, AKO mice and age-matched AMPKα1/α2-floxed littermates were fed a high-fat diet. At 14 weeks of age, the mice were divided randomly into different groups and treated with vehicle or C29 (30 $mg{\cdot}kg^{-1}{\cdot}day^{-1}$, p.o.) for another 14 weeks. At the end of the study, tissues were collected, weighed and stored at −80 °C.

Metabolic studies

Mouse body composition (including fat mass, lean mass, and fluid content) was determined using ^{1}H-nuclear magnetic resonance (NMR) spectroscopy (Minispec LF90 II, Bruker, Karlsruhe, Germany). For measurements of whole-body energy expenditure and O_2 consumption, mice were placed in metabolic chambers and monitored using a TSE PhenoMaster caging system (TSE Systems, Bad Homburg, Germany). Mice were intraperitoneally injected with the β3-adrenergic receptor-specific agonist CL316,243 (C5976-5MG, Sigma-Aldrich, St. Louis, MO, USA) (1 mg/kg) after a 12-h light/dark cycle to obtain the basal metabolic parameters. For cold exposure, mice were single-caged and exposed to a temperature of 4 °C for 6 h. Rectal temperature was monitored every hour using a BAT-12 microprobe digital thermometer and RET-3 mouse rectal probe (Physitemp Instruments, Clifton, NJ, USA). Thermo images were taken using an E6 Thermal Imaging Infrared Camera (E6, FLIR Systems, Portland, OR, USA) at 6 h, and the interscapular skin temperature was analyzed using FLIR Tools software. For the oral glucose tolerance test (OGTT) and insulin tolerance test (ITT), mice were injected with glucose (2 g/kg) or insulin (0.75 U/kg) after starvation for 6 h, and blood glucose levels were detected with a glucometer at 0, 15, 30, 60, 90, and 120 min post-injection. The liver triacylglycerol (TG) and cholesterol (TC) contents were measured following a Folch extraction [32]. For TG and TC assays, the dried lipid residues were then dissolved in 800 μL of ethanol with 1% Triton. The kits used were as follows: TG (1.02.1801, Shanghai Fosun Long March Medical Science Co., Shanghai, China) and TC (1.02.0401, Shanghai Fosun Long March Medical Science Co., Shanghai, China). The kits used to measure plasma parameters were as follows: ALT (290703, 290704, Sysmex, Shanghai, China), AST (290705, 290706, Sysmex, Shanghai, China), CREA (290721, 290722, Sysmex, Shanghai, China), and BUN (290707, 290708, Sysmex, Shanghai, China).

Histology

Mouse tissues were fixed in 4% paraformaldehyde and embedded in paraffin. Sections were stained using hematoxylin and eosin (H&E) according to the manufacturer's instructions. The slides were examined under a Leica DM6 B microscope at the indicated magnification, and images were captured by a sCMOS camera under the same parameter setting. Quantification of HE-stained images was performed using ImageJ Software (National Institutes of Health, Bethesda, MD, USA).

Tissue distribution assay

HFD-fed mice were p.o. injected with a single dose of C29 (30 mg/kg). After 6 h, the animals were sacrificed, and tissue samples were collected and preserved at −80 °C. The compound concentration was determined by the liquid chromatography-mass spectrometry/mass spectrometry (LC-MS/MS) system (an Agilent 1200 HPLC coupled to an Agilent 6460 Triple Quad instrument, Agilent Technologies, Santa Clara, CA, USA). Data were analyzed by MassHunter Quantitative Analysis (version B.02.01, Agilent Technologies, Santa Clara, CA, USA).

Cell culture

Stromal vascular fraction (SVF) cells from adipose tissue were isolated as previously described [31]. Cells were maintained in DMEM/F12 (12400024, Gibco, Waltham, MA, USA) containing 10% FBS (10091-148, Gibco, Waltham, MA, USA) and 1% penicillin/streptomycin (0242,0382, VWR Life Science, PA, USA). Differentiation was induced by incubating the cells in growth medium supplemented with 850 nM insulin (Novolin, Changzheng Hospital, Shanghai, China), 0.5 mM 3-isobutyl-1-methylxanthine (IBMX) (I5879, Sigma-Aldrich, St. Louis, MO, USA), 1 μM dexamethasone (D4902, Sigma-Aldrich, St. Louis, MO, USA), 125 nM indomethacin (I7378, Sigma-Aldrich, St. Louis, MO, USA) and 1 nM 3,3′,5-triiodo-*L*-thyronine (T3) (T2877, Sigma-Aldrich, St. Louis, MO, USA) for 2 days. Then, the cells were transported to growth medium with 850 nM insulin and 1 nM T3. The medium was changed every 2 days. On day 7, the differentiated SVF cells were treated with

DMSO or C29 at the indicated concentration for 24 h, and further analysis was performed afterwards.

Quantitative RT-PCR analysis

Total RNA isolated from cells or homogenized tissues was lysed using TRIzol reagent (9019, TaKaRa, Japan). Reverse transcription was performed using PrimeScript Reverse Transcriptase (RR036, Takara, Japan) according to the manufacturer's instructions. The cDNA was amplified using 2× SYBR Green qPCR Master Mix (B21702, Bimake, Houston, TX, USA) and a Stratagene Mx3005P instrument (Agilent Technologies, Santa Clara, CA, USA). Relative mRNA expression was normalized to 36b4 measured in each sample. The primer sequences used in this study are listed in Supplementary Table S1.

Western blotting

Total proteins from cells or tissues were extracted with RIPA lysis buffer (P0013B, Beyotime, Haimen, China) and denatured with loading buffer. Equal amounts of protein per sample were loaded on SDS-PAGE gels and transferred onto nitrocellulose membranes (10600002, GE Healthcare, Little Chalfont, Buckinghamshire, UK). Membranes were blocked with 5% skim milk and incubated with different primary antibodies overnight followed by incubation with a secondary antibody. Details for the primary antibodies used are as follows: AMPKα (2532), phospho-AMPKα (Thr172) (2535), ACC (3662), phospho-ACC (Ser79) (3661) (Cell Signaling Technology, Trask Lane Danvers, MA, USA); UCP-1 (A5857, ABclonal, Wuhan, China), PGC-1α (ST1202, Calbiochem, Darmstadt, Germany), and β-actin (AM1021B, Abgent, San Diego, CA, USA). The blots were examined with ECL (RPN2232, GE Healthcare, Little Chalfont, Buckinghamshire, UK), and densitometry was performed by ImageJ Software (National Institutes of Health, Bethesda, MD, USA).

Statistical analysis

Data are expressed as the mean ± SEM, and significance was defined as $P < 0.05$ and determined by one-tailed Student's t test or one-way ANOVA followed by Dunnett's multiple comparisons test. All analyses were performed in GraphPad Prism (version 7.00, GraphPad Software, La Jolla, CA, USA).

RESULTS

AMPK allosteric activator C29 increases thermogenesis in differentiated iWAT-SVF cells

AMPK is well known as a cellular energy sensor, and its role in regulating the metabolic activity of brown and beige adipose tissue was recently identified [33]. C29 has been reported to be a novel allosteric AMPK activator [25]. To explore the effects of C29-induced AMPK activation on adipocyte thermogenesis, we used differentiated SVF cells from iWAT as a cell model. iWAT-SVF cells were induced to differentiate into beige adipocytes and then treated with DMSO or C29 at the indicated concentration on day 7 for 24 h. In differentiated iWAT-SVF cells, C29 treatment promoted the expression levels of thermogenesis markers such as *Ucp1*, peroxisome proliferator-activated receptor gamma coactivator 1-alpha (*Pgc-1a*), type II iodothyronine deiodinase *(Dio2)*, PR domain containing 16 (*Prdm16*), cytochrome *c* oxidase polypeptide 7a1 *(Cox7a1)*, cytochrome *c* oxidase polypeptide 8b *(Cox8b)*, elongation of very-long-chain fatty acids protein 3 *(Elovl3)* and cell death-inducing DFFA-like effector a (*Cidea*) in a dose-dependent manner (Fig. 1a). Fatty acid oxidation (FAO) genes, including carnitine palmitoyltransferase 1*a* (*Cpt1a*), long-chain acyl-CoA dehydrogenase (*Lcad*) and peroxisome proliferator-activated receptor *α* (*Ppara*), were also dramatically increased by C29 treatment compared to those in the control condition (Fig. 1a). The expression of beige-selective genes, such as TNF receptor superfamily member 9 (*Cd137*), transmembrane protein 26 (*Tmem26*), solute carrier family 27 member 1 (*Slc27a1*) and T-box transcription factor 1 (*Tbx1*), increased with a similar tendency (Fig. 1a). Moreover, the protein expression of UCP1 and PGC-1α was also markedly increased by C29 treatment, which was accompanied by the activation of AMPK in differentiated iWAT-SVF cells (Fig. 1b, c). These results suggest that C29 promotes mature beige adipocyte thermogenesis in vitro.

To further determine whether energy metabolism changed upon exposure to C29, a Seahorse instrument was used to perform cellular bioenergetic measurements on iWAT-SVF cells. The basal and uncoupled oxygen consumption rates (OCRs) of C29-treated adipocytes remained higher than those of untreated cells in a concentration-dependent manner (Fig. 1d, e). These data indicate that C29 promotes thermogenesis in differentiated iWAT-SVF cells together with the activation of AMPK.

Chronic C29 treatment ameliorates HFD-induced obesity and insulin resistance

To examine the therapeutic potential of C29 on diet-induced obesity in vivo, C57BL/6J male mice were fed a high-fat diet for 8 weeks and subsequently treated with vehicle or C29 (30 $mg{\cdot}kg^{-1}{\cdot}day^{-1}$, p.o.) for 9 weeks. After 4 weeks, the average body weight of C29-treated mice was significantly lower than that of the vehicle-treated control mice (Fig. 2a) without affecting appetite (Fig. 2b). We also analyzed the changes in fat mass and lean mass after the treatment. A significant reduction in fat mass after C29 administration (Fig. 2c) was observed, and the animals exhibited lower adiposity than the vehicle control mice. The relative iWAT and epididymal white adipose tissue (eWAT) weights were decreased in mice treated with C29, but the perirenal white adipose tissue (pWAT), BAT and liver weights were unchanged (Fig. 2d).

We further examined whether the reduced body weight gain caused by C29 treatment leads to an improvement in systemic glucose homeostasis. The fasting blood glucose level was decreased by C29 treatment (Supplementary Fig. S1a). Moreover, the oral glucose tolerance test (OGTT) showed that mice treated with C29 exhibited significantly lower blood glucose levels than vehicle-treated mice. (Supplementary Fig. S1b, c). This improvement was associated with moderate but significant increases in insulin sensitivity, as shown by insulin tolerance tests (ITT) (Supplementary Fig. S1d, e), indicating greater insulin sensitivity in the C29-treated mice. Furthermore, the plasma concentrations of alanine aminotransferase (ALT), aspartate aminotransferase (AST), creatinine (CREA) and urea nitrogen (BUN), which are indicators of liver and kidney damage, were significantly reduced after C29 treatment (Supplementary Fig. S1f–i). These results demonstrate that the anti-obesity roles of C29 are not due to its toxicity. Taken together, these results indicate that C29 reduces body weight and improves glucose tolerance and insulin sensitivity in HFD-fed mice.

C29 stimulates energy expenditure and improves cold tolerance

Since C29-treated mice consumed the same number of calories as control mice, the leanness in C29-treated mice was likely due to increased energy expenditure rather than decreased food intake. This was further demonstrated by increased oxygen consumption (VO_2) (Fig. 3a, b) and energy expenditure (EE) (Fig. 3c, d) under basal conditions and in response to the stimulation of the β3-adrenergic receptor agonist CL316,243, with unchanged locomotor activity (Supplementary Fig. S2b). Additionally, the respiration exchange ratio (RER) was slightly decreased in C29-treated mice under CL316,243 stimulation (Supplementary Fig. S2a).

To further examine the effects of C29 on adaptive thermogenesis, a cold tolerance test was performed and determined by rectal temperature and infrared imaging of heat intensity. C29 administration caused the exhibition of significantly higher core body temperature during the 6 h of 4 °C cold exposure (Fig. 3e).

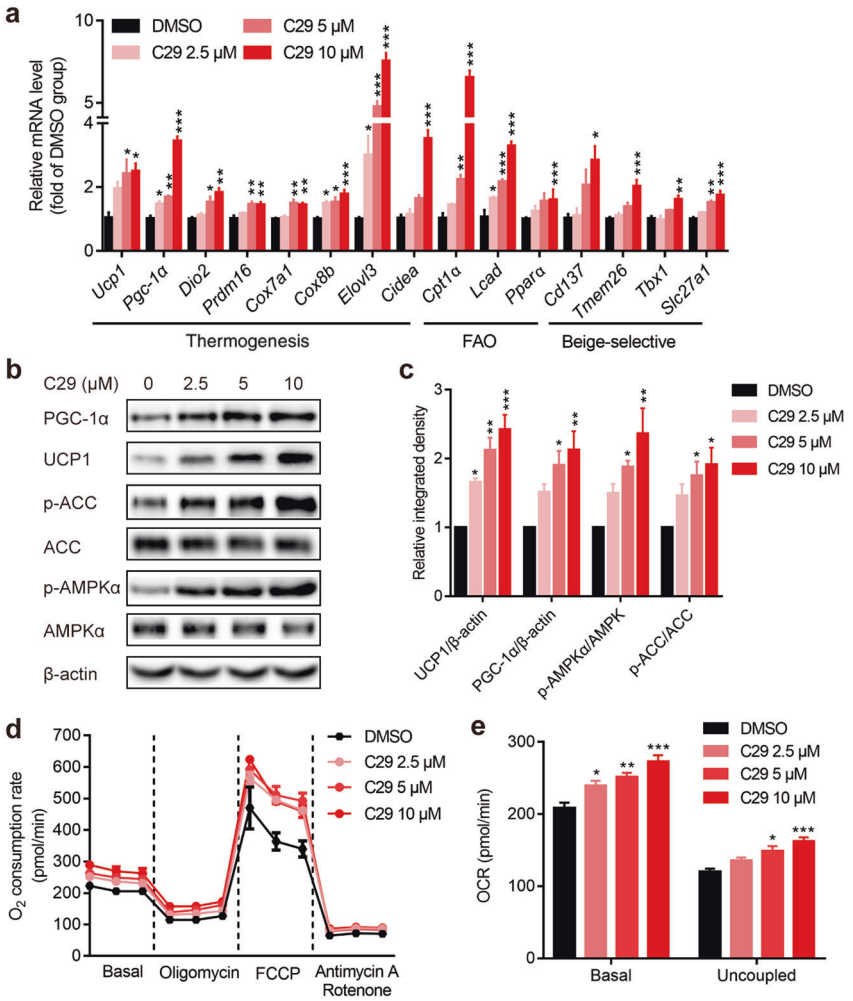

Fig. 1 C29 increased thermogenesis in differentiated iWAT-SVF cells. iWAT-SVF cells were induced to differentiate towards brown-like adipocytes and then treated with C29 at the indicated concentration for 24 h on day 7. Relative mRNA level of the indicated genes (**a**); Western blot analysis of the indicated proteins (**b, c**); β-actin was used as the loading control; basal and uncoupled cellular oxygen consumption rate (OCR) (**d, e**). $n = 3$. Data are the means ± SEM. $^{*}P < 0.05$, $^{**}P < 0.01$, $^{***}P < 0.001$, C29 group versus vehicle group by one-way ANOVA.

Additionally, the interscapular BAT skin temperature at 6 h was also markedly increased by C29 treatment (Fig. 3f, g). Together, these data suggest that the anti-obesity effects of C29 on HFD-fed mice might be due to increased energy expenditure.

C29-treated mice exhibit enhanced browning of iWAT

Because brown and beige adipose tissues are important regulators of energy expenditure [11], changes in the morphology of different adipose depots and related gene expression were observed to analyze the effects of C29 on adipose tissues. H&E staining showed that inguinal WAT depots from C29-treated mice had smaller adipocyte sizes, as indicated by a decreased adipocyte area (Fig. 4a, b). In agreement, the expression of thermogenesis-related genes, such as *Ucp1*, *Pgc-1α*, *Dio2*, *Prdm16*, *Cox7a1*, *Cox8b*, and *Elovl3*, was markedly enhanced in iWAT from C29-treated mice (Fig. 4e). Furthermore, the expression of genes related to FAO, including *Cpt1a*, *Lcad* and *Ppara*, was also significantly increased in iWAT (Fig. 4e). Consistent with this, Western blot results showed a higher level of UCP1 and PGC-1α expression, suggesting a conversion of iWAT into beige adipose tissue induced by C29 (Fig. 4f, g). This was accompanied by AMPK signaling activation, as evidenced by the increased phosphorylation of AMPKα and its downstream substrate acetyl-CoA carboxylase (ACC) (Fig. 4f, g). Moreover, the lipid droplets were unchanged in the BAT of C29-treated mice (Fig. 4c), whereas there was a moderate increase in the gene expression of *Pgc-1α, Prdm16*, *Cpt1a* and *Lcad* in BAT (Fig. 4h). However, the adipocyte area and expression of thermogenesis markers in eWAT were unaltered (Fig. 4c, i). These results indicate that C29 specifically induces browning in the iWAT of HFD-induced obese mice.

AMPK activation is indispensable to the prevention of HFD-induced obesity through C29

Next, we questioned whether C29 exerts its effects on high-fat diet-induced obesity mainly through its activation of adipocyte AMPK. Adipose-specific AMPKα1/α2 knockout (referred to as AKO) mice and age-matched floxed littermates were given a high-fat diet for 8 weeks and then treated with C29 or vehicle during the last 14 weeks of the diet. Consistent with our previous studies [31], AKO mice exhibited more obesity and greater adiposity than floxed mice, as evidenced by increased body weight, fat mass, iWAT weight, and pWAT weight (Fig. 5a, c, d). C29 treatment markedly reduced the body weight, fat mass, iWAT weight, and eWAT weight in floxed mice but did not affect those of AKO mice (Fig. 5a, c, d). Food intake was unaltered by C29 in both genotypes (Fig. 5b). These results indicate that C29 ameliorates HFD-induced obesity in an AMPK-dependent manner.

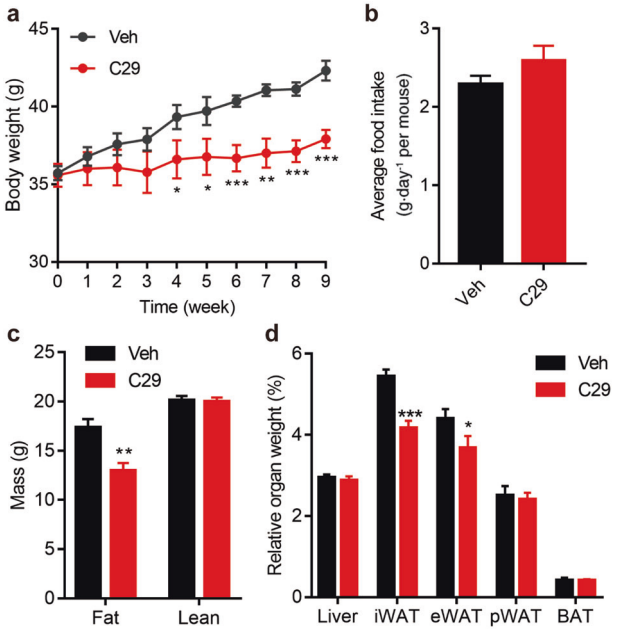

Fig. 2 Chronic C29 treatment reduced high-fat diet-induced obesity. Body weight (**a**) and average food intake per day (**b**) in high-fat diet-fed mice during 9 weeks of treatment. Fat and lean mass (**c**) and relative weight of the liver and different adipose tissue depots (**d**) after treatment. $n = 6$. Data are the means ± SEM. $^{*}P < 0.05$, $^{**}P < 0.01$, $^{***}P < 0.001$, C29 group versus vehicle group by Student's t test.

Diet-induced obesity is frequently associated with glucose intolerance and progressive metabolic dysfunction. In line with our previous results, AKO mice displayed a marked exacerbation in glucose homeostasis and insulin sensitivity relative to their age-matched floxed littermates (Supplementary Fig. S4a–d). C29 treatment improved glucose tolerance in both AKO and floxed mice, although the GTT AUC in AKO mice was decreased by 20% compared with 7% in floxed mice (Supplementary Fig. S4a, b). Furthermore, C29 treatment also improved insulin sensitivity in both genotypes, as the ITT AUC decreased by 19% in AKO mice and by 11% in floxed mice (Supplementary Fig. S4c, d). Our previous study reported that treatment with C29 improved lipid metabolism in the liver of *ob/ob* mice by increasing hepatic AMPK activity [25]. In agreement, C29 markedly reduced the liver TG and TC contents in both HFD-fed AKO and floxed mice (Supplementary Fig. S4e, f). Since hepatic steatosis is one of the hallmarks of insulin resistance and metabolic dysfunction [34], the reduction in the AUC of the GTT and ITT in AKO mice may be partially due to the role of C29 in the liver. These data indicate that the improvement in the metabolic profiles of HFD-induced obese mice through C29 is at least partially dependent on adipose AMPK.

C29 increases energy expenditure and maintains body temperature during cold exposure in an AMPK-dependent manner

To further examine the differences in energy expenditure among these genotypes, metabolic studies were performed in AKO mice and age-matched floxed littermates treated with the vehicle or C29 and observed by indirect calorimetry. Under basal conditions or after i.p. injections with the β3-AR activator CL316,243, AKO mice exhibited a significantly lower oxygen consumption rate (VO_2) or energy expenditure (EE) compared to age-matched floxed mice (Fig. 6a–d). Consistent with previous studies, floxed mice treated with C29 showed a higher oxygen consumption rate (VO_2) and energy expenditure (EE) (Fig. 6a–d). Importantly, the increases in VO_2 and EE levels by C29 were completely blunted in AKO mice (Fig. 6a–d), suggesting that a large part of the increased oxygen consumption rate and energy expenditure by C29 depends on adipocyte AMPKα. Furthermore, C29 treatment displayed a mild decrease in the respiratory exchange ratio (RER) in floxed mice but not in AKO mice under CL316,243 injection (Supplementary Fig. S5a). Additionally, spontaneous locomotor activity did not significantly differ among the four groups (Supplementary Fig. S5b).

Moreover, during the 6 h of cold exposure at 4 °C, AKO mice were unable to maintain their core body temperature (Fig. 6e) or interscapular BAT temperature (Fig. 6f, g) compared with the age-matched floxed mice. The C29-administered floxed mice showed a relatively higher body temperature and skin temperature surrounding the BAT; however, this effect was absent in AKO mice (Fig. 6e–g). Overall, these findings implicate a significant effect of adipocyte AMPKα that can be attributed to C29-promoted energy expenditure and improved cold tolerance. These results support the fact that C29 enhances energy expenditure and maintains body temperature through activation of the AMPK signaling pathway.

C29 induces browning in the iWAT of HFD-fed mice through the activation of AMPK

Histological analysis revealed a larger adipocyte size in iWAT (Fig. 7a, b), and this was consistent with the markedly diminished expression of thermogenesis-related and FAO-related genes in the iWAT of AKO mice (Fig. 7c). We also observed larger lipid droplets accumulated in the BAT of AKO mice (Supplementary Fig. S6a, b), which was probably because of the decreased expression of FAO-related genes and some thermogenic genes, such as *Pgc-1α* and *Prdm16*, in the BAT (Supplementary Fig. S6e). Because C29 treatment significantly decreased the adipocyte area (Fig. 7a, b) and induced the expression of thermogenesis and FAO-related genes in the iWAT of floxed mice, it was unchanged when AMPKα was deleted (Fig. 7c and Supplementary Fig. S6c). Similar results were observed in the protein expression levels of UCP1 and PGC-1α (Fig. 7d, e). Additionally, C29 slightly increased some of the thermogenic genes in the BAT of floxed mice but not in AKO mice (Supplementary Fig. S6d, e), although the decrease in lipid droplets in BAT did not reach statistical significance (Supplementary Fig. S6a, b). These results indicate that adipose AMPK activation is essential for C29-facilitated thermogenesis in iWAT.

DISCUSSION

Over the past years, the ability of classical brown and beige adipocytes to maintain energy homeostasis has roused great interest. Targeting energy expenditure has represented an effective method for obesity therapies. Despite their common ability to produce heat, brown and beige adipocytes have different features and should be regarded as distinct cell types. Beige adipocytes have a greater inducibility towards UCP1 expression and a higher capacity for thermogenesis upon stimulation compared to classical brown adipocytes [8]. More fundamentally, beige adipocytes have a distinct embryological origin compared to brown adipocytes. Classical BAT comes from the myogenic factor 5^{+} ($Myf5^{+}$) lineage shared with skeletal muscle, while lineage tracing analysis describes beige adipocytes as coming from the iWAT, which is derived from $Myf5^{-}$ precursor cells [7, 35]. Some populations of precursors can be induced by cold and adrenergic stimulation to develop into beige adipocytes. A number of studies have indicated that early B-cell factor 2^{+} ($EBF2^{+}$) platelet-derived growth factor receptor-α^{+} ($PDGFR\alpha^{+}$) precursor cells, $PDGFR\beta^{+}$ mural cells and myosin heavy chain 11^{+} ($MYH11^{+}$) smooth muscle $actin^{+}$ (SMA^{+})

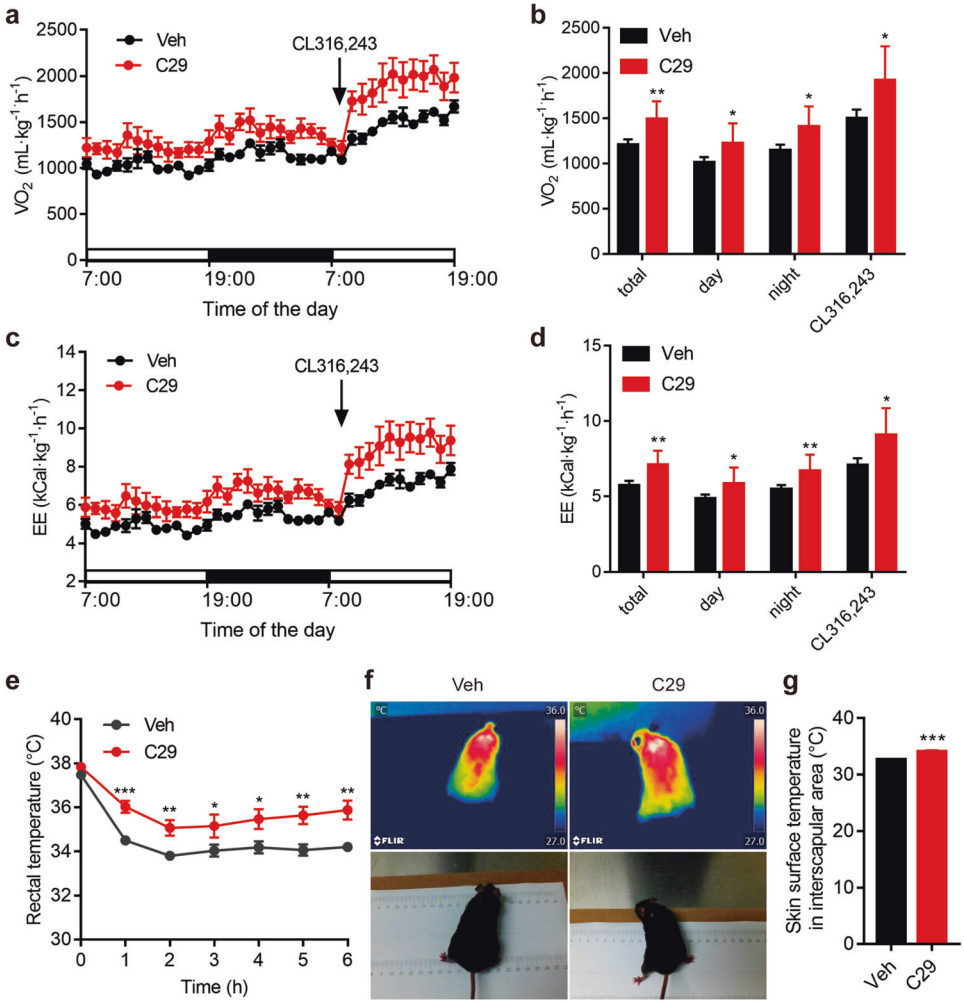

Fig. 3 C29 promoted energy expenditure and adaptive thermogenesis. The change in O_2 consumption (VO_2) (**a**), change in energy expenditure (EE) (**c**), average O_2 consumption (VO_2) (**b**) and energy expenditure (EE) (**d**) under basal and CL316,243 stimulation conditions after 7 weeks of treatment. Body temperature change (**e**), representative thermal images of mice (**f**) and interscapular BAT skin temperature (**g**) during cold exposure at 4 °C for 6 h after 8 weeks of treatment. $n = 6$. Data are the means ± SEM. $^*P < 0.05$, $^{**}P < 0.01$, $^{***}P < 0.001$, C29 group versus vehicle group by Student's *t* test.

smooth muscle cells can be recruited and differentiated into beige adipocytes [36–39]. Our findings showed that C29 selectively promotes the browning of iWAT, as indicated by the increased expression of thermogenic genes and proteins both in vitro and in vivo, together with the activation of AMPK (Fig. 1b, 4f).

Although the interscapular skin temperature was higher in C29-treated mice (Fig. 3f), the tissue weight and size of lipid droplets were unaltered, and only a slight increase in thermogenic and FAO genes was detected in BAT (Fig. 4a, b, f). These findings were consistent with the finding that treatment with C29 did not result in enhanced thermogenesis in mature brown adipocytes from BAT (data not shown). The different embryonic origins of brown and beige adipocytes [6] might be the cause of the discrepant effects of C29, suggesting that C29 might play distinctive roles in affecting these two thermogenic cells. In addition, it has been reported that some WAT depots are less susceptible to browning [40, 41]. Treatment with C29 did not alter the expression of thermogenic genes in eWAT, a finding that is consistent with reports that eWAT has a lower potential for browning than iWAT. In addition, C29 plays a critical role in regulating cold tolerance and energy expenditure, which are associated with promoting browning in iWAT. Furthermore, the reduced body weight gain and iWAT and eWAT weights are consistent with the phenomenon in C29-treated *ob/ob* mice that we previously reported [25], indicating the potential of C29 in anti-obesity therapies.

Numerous studies have reported that some indirect AMPK activators could improve whole-body energy metabolism and anti-obesity. For example, metformin induces the browning of WAT, which has a beneficial effect on obesity [27]. Berberine can promote thermogenesis in BAT and WAT via the AMPK-PGC-1α pathway [28]. However, the indirect pharmacological activation of AMPK might cause off-target effects [42]. Moreover, the pan-AMPK activator O304 can increase energy expenditure and BAT metabolic activity [29]. In our previous study, we also found that the specific AMPKβ1 agonist A-769662 promoted thermogenesis in differentiated iWAT-SVF cells, which was AMPK-dependent [31]. Reduced AMPK activity in adipose tissue is well known to be associated with obesity [43, 44]. However, it is worth noting that the direct reliance on the activation of adipose tissue AMPK has not been shown to be involved in most of these studies, especially those performed in vivo. As C29 has been indicated to be an AMPK activator, we therefore

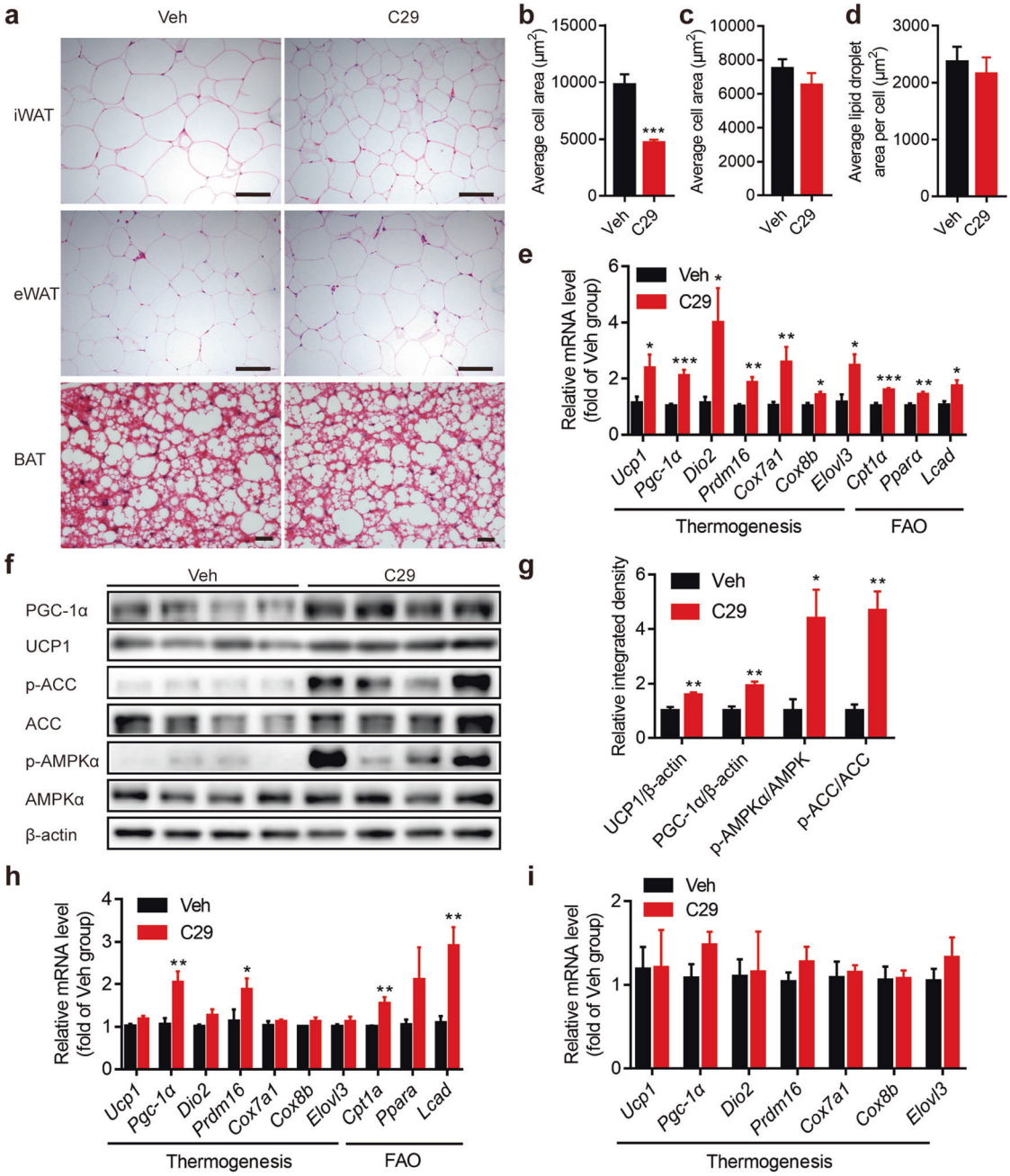

Fig. 4 C29 induced the browning of iWAT in HFD-induced mice. Representative H&E-stained images of iWAT (top), eWAT (middle) and BAT (bottom) after treatment, scale bar, 100 μm (**a**). The average adipocyte area of iWAT (**b**) and eWAT (**c**) and average lipid droplet area of BAT (**d**) after treatment, $n = 6$. Relative mRNA levels of the indicated genes (**e**) and Western blot analysis of the indicated proteins (**f, g**) in iWAT; β-actin was used as the loading control, $n = 4$–6. Relative mRNA levels of the indicated genes in BAT (**h**) and eWAT (**i**) after treatment. $n = 6$. Data are the means ± SEM. $^{*}P < 0.05$, $^{**}P < 0.01$, $^{***}P < 0.001$, C29 group versus vehicle group by Student's t test.

hypothesized that C29 may promote energy expenditure and protect against HFD-induced obesity through the activation of AMPK in adipose tissue.

To specifically investigate the role of adipocyte AMPK in the ability of C29 to protect against diet-induced metabolic dysfunction, adipocyte-specific AMPK KO mice were utilized, and we found that the reduced body weight (Fig. 5a), enhanced energy expenditure (Fig. 6c, d) and cold tolerance (Fig. 6e) as a result of C29 treatment were not observed in AKO mice, indicating that adipose AMPK plays a core role in C29's effects on the regulation of the organismal energy balance. PGC-1α is a critical transcriptional coactivator involved in the adaptive thermogenic program that can stimulate UCP1 expression. However, PGC-1α is required for AMPK to regulate mitochondrial homeostasis either by direct phosphorylation or by increasing its expression [45, 46]. It has been reported that the AMPK indirect activator berberine promotes thermogenesis in brown and beige adipocytes via the AMPK-PGC-1α pathway [28]. Another consistent finding is that AKO mice showed a reduced total number of mitochondria in iWAT and BAT, indicating that adipocyte AMPK deficiency impaired mitochondrial biogenesis [31]. We found that the increase in the

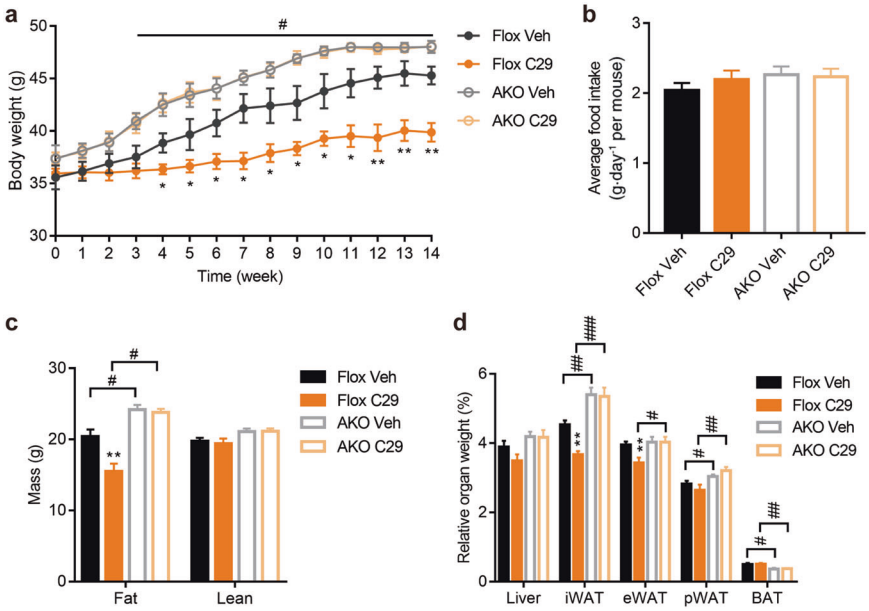

Fig. 5 C29 protected against HFD-induced obesity in an AMPK-dependent manner. Body weight (**a**) and average food intake per day (**b**) in HFD-fed AKO mice and age-matched floxed littermates during 14 weeks of treatment. Fat and lean mass (**c**) and relative weight of the liver and different adipose tissue depots (**d**) after treatment. $n = 6$. Data are the means ± SEM. $^{*}P < 0.05$, $^{**}P < 0.01$, C29 group versus vehicle group; $^{\#}P < 0.05$, $^{\#\#}P < 0.01$, $^{\#\#\#}P < 0.001$ AKO group versus floxed group by Student's *t* test.

thermogenic markers UCP1 and PGC-1α after C29 treatment was absent in AKO mice (Fig. 6c, d), suggesting that PGC-1α might be vital for C29 function in the browning of iWAT and that the AMPK-PGC-1α axis is necessary for the UCP1-dependent thermogenic effects of C29. Compared to other indirect or direct AMPK activators, C29 allosterically activates AMPK depending on the direct activation of the AMPK kinase domain with the nonselective property of heterotrimers. C29 has shown abundant distribution in adipose tissue as well as direct reliance on the activation of adipose tissue AMPK for the anti-obesity effects. These findings show that C29 might be a new potential AMPK activator for the treatment of obesity and related metabolic disorders.

In addition to modulating mitochondrial biogenesis, AMPK also controls mitophagy through the phosphorylation of ULK1, which can maintain mitochondrial quality through the clearance of damaged mitochondria [47]. A previous study reported that the adipose tissue-specific deletion of AMPK β1/β2 subunits impaired the mitochondrial structure in BAT, a finding that is consistent with the reduction in the phosphorylation of ULK1 [24]. Future studies are needed to confirm whether adipocyte AMPK activation by C29 could affect mitophagy through ULK1.

It should be noted that other UCP1-independent mechanisms are involved in beige fat thermogenesis, such as creatine-driven substrate cycling [48] and Ca^{2+} cycling via the sarco/endoplasmic reticulum Ca^{2+}-ATPase 2b (SERCA2b)-ryanodine receptor 2 (RyR2) pathway [49]. Recent reports have suggested that in HFD-fed mice, AMPK activation induced a switch in iWAT towards a skeletal muscle-like phenotype, which was UCP1-independent. Consistent with this, we also found that the absence of AMPK counteracted the expression of the muscular gene *Serca* and reduced the SERCA-mediated Ca^{2+} cycle in beige adipocytes [50]. Hence, whether UCP1-independent noncanonical thermogenic mechanisms are involved in C29-induced thermogenesis in iWAT will require additional analyses to verify.

The amelioration of glucose homeostasis and insulin sensitivity is associated with enhanced glucose uptake in adult human BAT [51, 52]. Moreover, the expansion and activation of beige adipocytes have also been identified to improve glucose tolerance [41, 53]. Since C29 plays a minor role in the activation of brown adipocytes, we suggested that the significantly enhanced thermogenic activity of beige adipocytes rather than brown adipocytes contributed more to this process. In addition, glucose tolerance and insulin sensitivity were slightly improved in C29-treated AKO mice (Supplementary Fig. S4a–d), indicating that in addition to adipose tissue, other insulin-responsive tissues, such as muscle and liver, may also contribute to this phenotype. Recent studies have shown that the two potent pan-AMPK activators PF-739 and MK-8722, which activate AMPK in skeletal muscles, have resulted in increased glucose uptake, which causes an improvement in glucose homeostasis and insulin sensitivity in diabetic mice and nonhuman primates [54, 55]. In our previous studies [25], we reported that C29 could stimulate glucose uptake in an AMPK-dependent manner in L6 myotube cells. However, the activation of AMPK in the skeletal muscle of *ob/ob* mice after C29 treatment was weak. Furthermore, the distribution of C29 was poor in the skeletal muscle of both *ob/ob* mice and HFD-fed mice (Supplementary Fig. S3), which could not attain the effective concentration in vivo. Taken together, we inferred the slight role of C29 in skeletal muscle in vivo. Moreover, it is well established that hepatic triglyceride accumulation is highly associated with whole-body insulin resistance and that the activation of AMPK in the liver could suppress lipogenesis [43]. Therefore, the amelioration of insulin sensitivity may be partly due to the considerable distribution of C29 in the liver (Supplementary Fig. S3). Consistent with these findings, our previous study reported that C29 ameliorated lipid metabolism in hepatocytes and the liver of *ob/ob* mice due to its activation of hepatic AMPK [25]. Furthermore, we also found that hepatic triglyceride and cholesterol accumulation were decreased in both genotypes after C29 treatment (Supplementary Fig. S4e, f). More importantly, similar to other studies, we showed that mice lacking adipose tissue AMPK can also develop enhanced liver lipid accumulation and insulin resistance, which indicated that the abolishment of AMPK in adipose tissue may be one of the

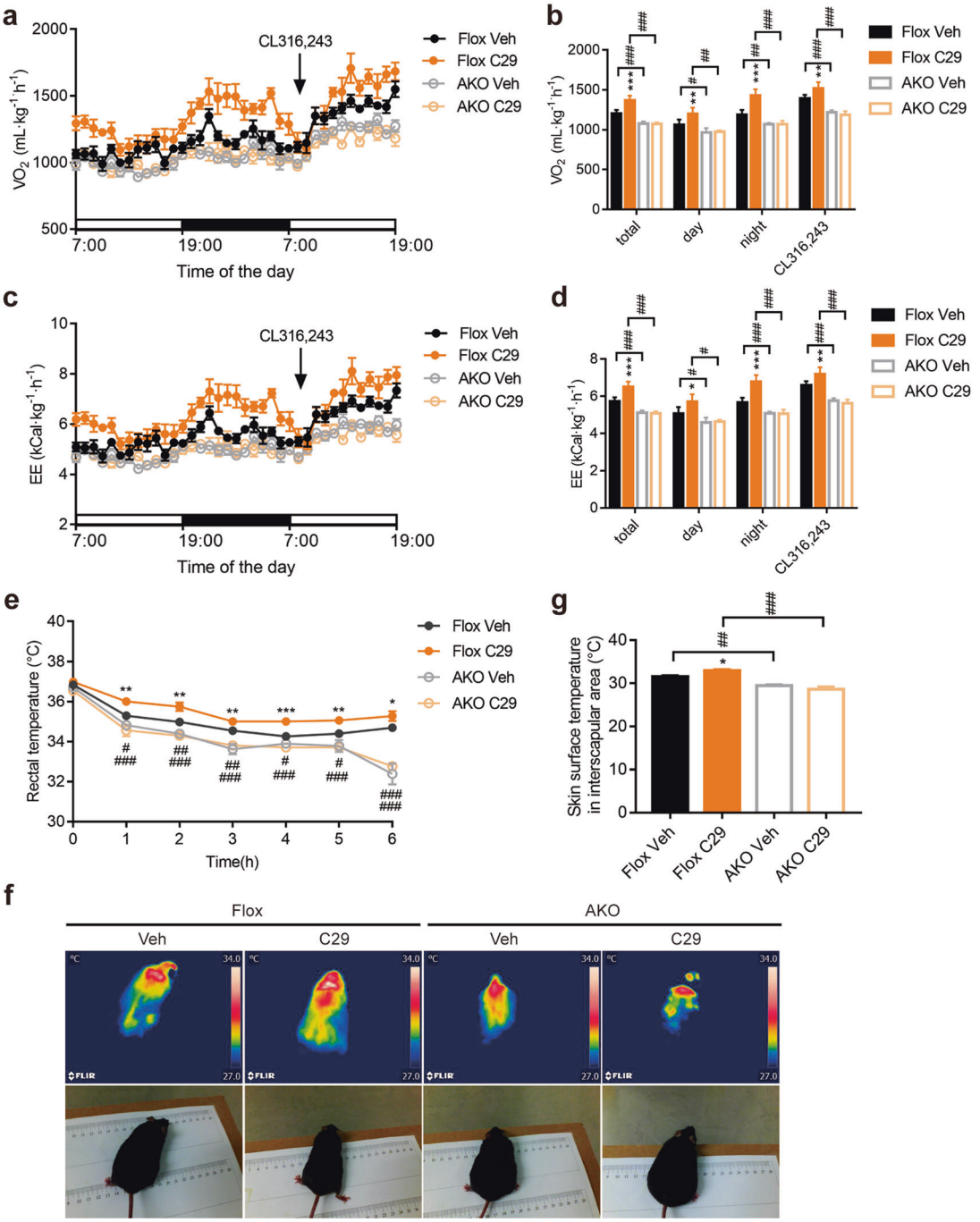

Fig. 6 C29 improved energy expenditure and cold tolerance through the activation of adipocyte AMPK. The change in O_2 consumption (VO_2) (**a**), change in energy expenditure (EE) (**c**), average O_2 consumption (VO_2) (**b**) and energy expenditure (EE) (**d**) under basal and CL316,243 stimulation conditions in HFD-fed AKO mice and age-matched floxed littermates after 10 weeks of treatment. Body temperature change (**e**), representative thermal images of mice (**f**) and interscapular BAT skin temperature (**g**) during cold exposure at 4 °C for 6 h after 12 weeks of treatment, $n = 5$. Data are the means ± SEM. $^{*}P < 0.05$, $^{**}P < 0.01$, $^{***}P < 0.001$, C29 group versus vehicle group; $^{\#}P < 0.05$, $^{\#\#}P < 0.01$, $^{\#\#\#}P < 0.001$, AKO group versus floxed group by Student's *t* test.

causes of insulin resistance (Supplementary Fig. S4e, f) [24, 31]. Given that AMPK activation could generate insulin-sensitizing effects [56], the activity of the insulin signaling pathway should be further studied to confirm the insulin resistance status after C29 treatment. Taken together, these data suggest that C29 treatments improved glucose tolerance and insulin sensitivity in HFD-induced obese mice, which are partly dependent on adipose AMPK.

In conclusion, our results provide evidence for the first time that a novel pyrazolone derivative called C29 improves thermogenesis in iWAT in a UCP1-dependent manner, contributing beneficial effects to weight loss and energy expenditure via the adipose AMPK-PGC-1α signaling pathway. These findings indicate that the activation of AMPK in adipose tissue might be a new potential target to protect against obesity and other metabolic dysfunctions.

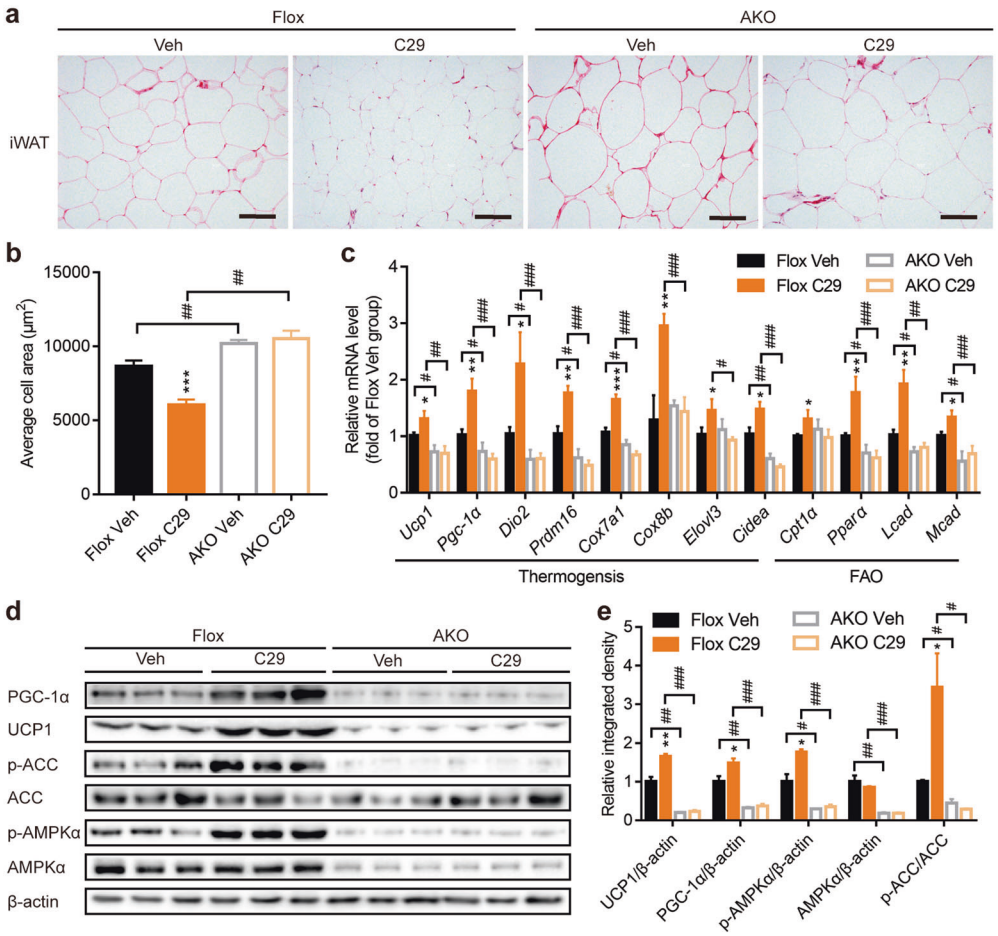

Fig. 7 AMPK activation was essential for C29 in the browning of iWAT in HFD-induced mice. Representative H&E-stained images of iWAT after treatment; scale bar, 100 μm (**a**). Average adipocyte area of iWAT in HFD-fed AKO mice and age-matched floxed littermates after treatment (**b**), $n = 6$. Relative mRNA levels of the indicated genes (**c**) and Western blot analysis of the indicated proteins (**d, e**) in iWAT; β-actin was used as the loading control, $n = 3–5$. Data are the means ± SEM. $^{*}P < 0.05$, $^{**}P < 0.01$, $^{***}P < 0.001$, C29 group versus vehicle group; $^{\#}P < 0.05$, $^{\#\#}P < 0.01$, $^{\#\#\#}P < 0.001$, AKO group versus floxed group by Student's *t* test.

ACKNOWLEDGEMENTS

This work was supported by grants from the National Natural Science Foundation of China (No. 81470166 and 81273566) and the National Science & Technology Major Project "Key New Drug Creation and Manufacturing Program" of China (2018ZX09711002).

AUTHOR CONTRIBUTIONS

BHL contributed to the performance of experiments, analysis of the data, and writing of the manuscript. MZ contributed to the C29 preparation and analysis. YND, LS, and HWJ contributed to the performance of experiments. JL contributed to the discussion and provided professional advice. JYL and FJN contributed to the research design and review of the manuscript.

ADDITIONAL INFORMATION

The online version of this article (https://doi.org/10.1038/s41401-020-00524-0) contains supplementary material, which is available to authorized users.

Competing interests: The authors declare no competing interests.

REFERENCES

1. Wang YC, McPherson K, Marsh T, Gortmaker SL, Brown M. Health and economic burden of the projected obesity trends in the USA and the UK. Lancet. 2011;378:815–25.
2. Rosen ED, Spiegelman BM. Adipocytes as regulators of energy balance and glucose homeostasis. Nature. 2006;444:847–53.
3. Rosen Evan D, Spiegelman, Bruce M. What we talk about when we talk about fat. Cell. 2014;156:20–44.
4. Seale P, Lazar MA. Brown fat in humans: turning up the heat on obesity. Diabetes. 2009;58:1482–4.
5. Spiegelman BM. Banting lecture 2012: regulation of adipogenesis: toward new therapeutics for metabolic disease. Diabetes. 2013;62:1774–82.
6. Peirce V, Carobbio S, Vidal-Puig A. The different shades of fat. Nature. 2014;510:76–83.
7. Seale P, Bjork B, Yang W, Kajimura S, Chin S, Kuang S, et al. PRDM16 controls a brown fat/skeletal muscle switch. Nature. 2008;454:961–7.
8. Ishibashi J, Seale P. Medicine. Beige can be slimming. Science. 2010;328:1113–4.
9. Wu J, Boström P, Sparks LM, Ye L, Choi JH, Giang AH, et al. Beige adipocytes are a distinct type of thermogenic fat cell in mouse and human. Cell. 2012;150:366–76.
10. Cohen P, Spiegelman BM. Brown and beige fat: molecular parts of a thermogenic machine. Diabetes. 2015;64:2346–51.
11. Wang W, Seale P. Control of brown and beige fat development. Nat Rev Mol Cell Biol. 2016;17:691–702.
12. Boström P, Wu J, Jedrychowski MP, Korde A, Ye L, Lo JC, et al. A PGC1-α-dependent myokine that drives brown-fat-like development of white fat and thermogenesis. Nature. 2012;481:463–8.
13. Fisher FM, Kleiner S, Douris N, Fox EC, Mepani RJ, Verdeguer F, et al. FGF21 regulates PGC-1α and browning of white adipose tissues in adaptive thermogenesis. Genes Dev. 2012;26:271–81.
14. Bordicchia M, Liu D, Amri EZ, Ailhaud G, Dessi-Fulgheri P, Zhang C, et al. Cardiac natriuretic peptides act via p38 MAPK to induce the brown fat thermogenic program in mouse and human adipocytes. J Clin Invest. 2012;122:1022–36.

15. Boon MR, van den Berg SA, Wang Y, van den Bossche J, Karkampouna S, Bauwens M, et al. BMP7 activates brown adipose tissue and reduces diet-induced obesity only at subthermoneutrality. PLoS One. 2013;8:e74083.
16. Qian SW, Tang Y, Li X, Liu Y, Zhang YY, Huang HY, et al. BMP4-mediated brown fat-like changes in white adipose tissue alter glucose and energy homeostasis. Proc Natl Acad Sci USA. 2013;110:E798–E807.
17. Ohno H, Shinoda K, Spiegelman BM, Kajimura S. PPARγ agonists induce a white-to-brown fat conversion through stabilization of PRDM16 protein. Cell Metab. 2012;15:395–404.
18. Carling D. The AMP-activated protein kinase cascade-a unifying system for energy control. Trends Biochem Sci. 2004;29:18–24.
19. Grahame Hardie D. AMP-activated protein kinase: a key regulator of energy balance with many roles in human disease. J Intern Med. 2014;276:543–59.
20. Carling D, Mayer FV, Sanders MJ, Gamblin SJ. AMP-activated protein kinase: nature's energy sensor. Nat Chem Biol. 2011;7:512–8.
21. Hardie DG. AMPK: a key regulator of energy balance in the single cell and the whole organism. Int J Obes (Lond). 2008;32(Suppl 4):S7–S12.
22. Minokoshi Y, Alquier T, Furukawa N, Kim YB, Lee A, Xue B, et al. AMP-kinase regulates food intake by responding to hormonal and nutrient signals in the hypothalamus. Nature. 2004;428:569–74.
23. Steinberg GR, Kemp BE. AMPK in health and disease. Physiol Rev. 2009;89:1025–78.
24. Mottillo EP, Desjardins EM, Crane JD, Smith BK, Green AE, Ducommun S, et al. Lack of adipocyte AMPK exacerbates insulin resistance and hepatic steatosis through brown and beige adipose tissue function. Cell Metab. 2016;24:118–29.
25. Zhang M, Xie ZF, Zhang RT, Chen DK, Gu M, Cui SC, et al. Novel substituted pyrazolone derivatives as AMP-activated protein kinase activators to inhibit lipid synthesis and reduce lipid accumulation in ob/ob mice. Acta Pharmacol Sin. 2018;39:1622–32.
26. Gaidhu MP, Frontini A, Hung S, Pistor K, Cinti S, Ceddia RB. Chronic AMP-kinase activation with AICAR reduces adiposity by remodeling adipocyte metabolism and increasing leptin sensitivity. J Lipid Res. 2011;52:1702–11.
27. Kim EK, Lee SH, Jhun JY, Byun JK, Jeong JH, Lee SY, et al. Metformin prevents fatty liver and improves balance of white/brown adipose in an obesity mouse model by inducing FGF21. Mediators Inflamm. 2016;2016:5813030.
28. Zhang Z, Zhang H, Li B, Meng X, Wang J, Zhang Y, et al. Berberine activates thermogenesis in white and brown adipose tissue. Nat Commun. 2014;5:5493.
29. Steneberg P, Lindahl E, Dahl U, Lidh E, Straseviciene J, Backlund F, et al. PAN-AMPK activator O304 improves glucose homeostasis and microvascular perfusion in mice and type 2 diabetes patients. JCI Insight. 2018;3:e99114.
30. Zhang X, Zhang QX, Wang X, Zhang L, Qu W, Bao B, et al. Dietary luteolin activates browning and thermogenesis in mice through an AMPK/PGC1α pathway-mediated mechanism. Int J Obes (Lond). 2016;40:1841–9.
31. Wu L, Zhang L, Li B, Jiang H, Duan Y, Xie Z, et al. AMP-activated protein kinase (AMPK) regulates energy metabolism through modulating thermogenesis in adipose tissue. Front Physiol. 2018;9:122.
32. Folch J, Lees M, Sloane, Stanley GH. A simple method for the isolation and purification of total lipides from animal tissues. J Biol Chem. 1957;226:497–509.
33. Desjardins EM, Steinberg GR. Emerging role of AMPK in brown and beige adipose tissue (BAT): implications for obesity, insulin resistance, and type 2 diabetes. Curr Diab Rep. 2018;18:80.
34. Petersen MC, Shulman GI. Mechanisms of insulin action and insulin resistance. Physiol Rev. 2018;98:2133–223.
35. Sanchez-Gurmaches J, Hung CM, Sparks CA, Tang Y, Li H, Guertin DA. PTEN loss in the Myf5 lineage redistributes body fat and reveals subsets of white adipocytes that arise from Myf5 precursors. Cell Metab. 2012;16:348–62.
36. Wang W, Kissig M, Rajakumari S, Huang L, Lim HW, Won KJ, et al. Ebf2 is a selective marker of brown and beige adipogenic precursor cells. Proc Natl Acad Sci USA. 2014;111:14466–71.
37. Berry DC, Jiang Y, Graff JM. Mouse strains to study cold-inducible beige progenitors and beige adipocyte formation and function. Nat Commun. 2016;7:10184.
38. Vishvanath L, MacPherson KA, Hepler C, Wang QA, Shao M, Spurgin SB, et al. Pdgfrβ+ mural preadipocytes contribute to adipocyte hyperplasia induced by high-fat-diet feeding and prolonged cold exposure in adult mice. Cell Metab. 2016;23:350–9.
39. Long JZ, Svensson KJ, Tsai L, Zeng X, Roh HC, Kong X, et al. A smooth muscle-like origin for beige adipocytes. Cell Metab. 2014;19:810–20.
40. Waldén TB, Hansen IR, Timmons JA, Cannon B, Nedergaard J. Recruited vs. nonrecruited molecular signatures of brown, "brite," and white adipose tissues. Am J Physiol Endocrinol Metab. 2012;302:E19–31.
41. Seale P, Conroe HM, Estall J, Kajimura S, Frontini A, Ishibashi J, et al. Prdm16 determines the thermogenic program of subcutaneous white adipose tissue in mice. J Clin Invest. 2011;121:96–105.
42. Cool B, Zinker B, Chiou W, Kifle L, Cao N, Perham M, et al. Identification and characterization of a small molecule AMPK activator that treats key components of type 2 diabetes and the metabolic syndrome. Cell Metab. 2006;3:403–16.
43. Ruderman NB, Carling D, Prentki M, Cacicedo JM. AMPK, insulin resistance, and the metabolic syndrome. J Clin Invest. 2013;123:2764–72.
44. Xu XJ, Gauthier MS, Hess DT, Apovian CM, Cacicedo JM, Gokce N, et al. Insulin sensitive and resistant obesity in humans: AMPK activity, oxidative stress, and depot-specific changes in gene expression in adipose tissue. J Lipid Res. 2012;53:792–801.
45. Suwa M, Nakano H, Kumagai S. Effects of chronic AICAR treatment on fiber composition, enzyme activity, UCP3, and PGC-1 in rat muscles. J Appl Physiol. 1985;2003:960–8.
46. Jäger S, Handschin C, St-Pierre J, Spiegelman BM. AMP-activated protein kinase (AMPK) action in skeletal muscle via direct phosphorylation of PGC-1α. Proc Natl Acad Sci USA. 2007;104:12017–22.
47. Egan DF, Shackelford DB, Mihaylova MM, Gelino S, Kohnz RA, Mair W, et al. Phosphorylation of ULK1 (hATG1) by AMP-activated protein kinase connects energy sensing to mitophagy. Science. 2011;331:456–61.
48. Kazak L, Chouchani ET, Jedrychowski MP, Erickson BK, Shinoda K, Cohen P, et al. A creatine-driven substrate cycle enhances energy expenditure and thermogenesis in beige fat. Cell. 2015;163:643–55.
49. Ikeda K, Kang Q, Yoneshiro T, Camporez JP, Maki H, Homma M, et al. UCP1-independent signaling involving SERCA2b-mediated calcium cycling regulates beige fat thermogenesis and systemic glucose homeostasis. Nat Med. 2017;23:1454–65.
50. Aquilano K, Sciarretta F, Turchi R, Li BH, Rosina M, Ceci V, et al. Low-protein/high-carbohydrate diet induces AMPK-dependent canonical and non-canonical thermogenesis in subcutaneous adipose tissue. Redox Biol. 2020;36. https://doi.org/10.1016/j.redox.2020.101633.
51. Chondronikola M, Volpi E, Børsheim E, Porter C, Annamalai P, Enerbäck S, et al. Brown adipose tissue improves whole-body glucose homeostasis and insulin sensitivity in humans. Diabetes. 2014;63:4089–99.
52. Lee P, Smith S, Linderman J, Courville AB, Brychta RJ, Dieckmann W, et al. Temperature-acclimated brown adipose tissue modulates insulin sensitivity in humans. Diabetes. 2014;63:3686–98.
53. Kajimura S, Spiegelman BM, Seale P. Brown and beige fat: physiological roles beyond heat generation. Cell Metab. 2015;22:546–59.
54. Cokorinos EC, Delmore J, Reyes AR, Albuquerque B, Kjøbsted R, Jørgensen NO, et al. Activation of skeletal muscle AMPK promotes glucose disposal and glucose lowering in non-human primates and mice. Cell Metab. 2017;25:1147–1159.e10.
55. Myers RW, Guan HP, Ehrhart J, Petrov A, Prahalada S, Tozzo E, et al. Systemic pan-AMPK activator MK-8722 improves glucose homeostasis but induces cardiac hypertrophy. Science. 2017;357:507–11.
56. Coughlan KA, Valentine RJ, Ruderman NB, Saha AK. AMPK activation: a therapeutic target for type 2 diabetes? Diabetes Metab Syndr Obes. 2014;7:241–53.